Time-Resolved Ultraviolet Resonance Raman Studies of Protein Structure: Application to Bacteriorhodopsin†

James B. Ames,‡ Marianne Ros,‡ Jan Raap,§ Johan Lugtenburg,§ and Richard A. Mathies*,‡

Department of Chemistry, University of California, Berkeley, California 94720, and Department of Chemistry, Leiden University, 2300 RA Leiden, The Netherlands

Received January 10, 1992; Revised Manuscript Received March 31, 1992

ABSTRACT: Time-resolved ultraviolet resonance Raman spectra of bacteriorhodopsin are used to study protein structural changes on the nanosecond and millisecond time scales. Excitation at 240 nm is used to selectively enhance vibrational scattering from tyrosine so that changes in its hydrogen bonding and protonation state can be examined. Both nanosecond and millisecond UV Raman difference spectra indicate that none of the tyrosine residues change ionization state during the BR → K and BR → M transitions. However, intensity changes are observed at 1172 and 1615 cm^{-1} in the BR → M UV Raman difference spectra. The 1615-cm^{-1} feature shifts down 25 cm^{-1} in tyrosine-d_4-labeled BR, consistent with its assignment as a *tyrosine* vibration. The intensity changes in the BR → M UV Raman difference spectra most likely reflect an increase in resonance enhancement that occurs when one or more tyrosine residues interact more strongly with a hydrogen-bond acceptor in M_{412}. The frequency of the ν_{7a} feature (1172 cm^{-1}) in the BR → M UV Raman difference spectra supports this interpretation. The proximity of Tyr-185 and Asp-212 in the retinal binding pocket suggests that deprotonation of the Schiff base in M_{412} causes Tyr-185 to stabilize ionized Asp-212 by forming a stronger hydrogen bond.

Ultraviolet resonance Raman spectroscopy (UVRR)[1] is a powerful technique for probing protein structure (Asher, 1988; Harada & Takeuchi, 1986; Spiro & Grygon, 1988). Strong $\pi \rightarrow \pi^*$ electronic transitions in the ultraviolet by aromatic amino acid side chains (Figure 1) and by the amide group give rise to intense resonance Raman scattering. Selective resonance enhancement of the scattering from the amide group as well as from tyrosine, tyrosinate, and tryptophan residues can be achieved by properly selecting the excitation wavelength (Rava & Spiro, 1985a,b). UVRR has been used to study protein secondary structure (Harhay & Hudson, 1991; Song & Asher, 1988; Wang et al., 1991), side chain protonation state (Ames et al., 1990; Harada et al., 1990), hydrogen bonding (Hildebrandt et al., 1988; Miura et al., 1989), and protein/nucleotide interactions (Efremov et al., 1990; Toyama et al., 1991). Since Raman scattering is virtually instantaneous, UVRR should also be valuable in time-resolved studies of protein structural changes. Thus far, a relatively limited number of time-resolved UVRR studies of protein structure have been presented (Dasgupta et al., 1986; Kaminaka et al., 1990; Su et al., 1989). We therefore became interested in the possibility of using time-resolved UVRR to study protein structural changes in the bacteriorhodopsin photocycle.

Bacteriorhodopsin (BR), an intrinsic membrane protein found in *Halobacterium halobium*, functions as a light-driven proton pump (Mathies et al., 1991; Stoeckenius & Bogomolni, 1982). Absorption of a photon by the retinal prosthetic group triggers a photochemical reaction cycle: BR → J → K → L → M → N → O → BR. To elucidate the molecular mechanism of proton translocation in BR, structural changes of amino acid side chains during the photocycle must be characterized. FTIR and NMR spectroscopies have been used to probe the protonation state and environment of carboxylate (Braiman et al., 1988a; Engelhard et al., 1985, 1989) and aromatic residues (Braiman et al., 1988b; Herzfeld et al., 1990; Lin et al., 1987; McDermott et al., 1991). FTIR studies have also probed BR secondary structure (Earnest et al., 1990; Ormos, 1991) as well as the isomeric state of proline residues (Gerwert et al., 1990; Rothschild et al., 1990b). Site-specific mutagenesis has shown that Asp-85 and Asp-96 are critical in the proton pumping mechanism (Khorana, 1988; Mogi et al., 1988). In addition, UV absorption and FTIR studies have suggested that a tyrosine residue may play an important mechanistic role in the M_{412} intermediate (Dollinger et al., 1986; Hanamoto et al., 1984). More recently, FTIR studies on BR mutants have suggested that Tyr-185 is ionized in BR_{568} and in M_{412} and that it becomes protonated in K and in dark-adapted BR_{555} (Braiman et al., 1988b). However, recent solid-state NMR (Herzfeld et al., 1990) and UVRR studies (Ames et al., 1990) did not detect tyrosinate in BR_{568} nor a change of tyrosine ionization state between BR_{568} and BR_{555}. Additional work is needed to clarify the role of tyrosine in the photocycle.

Here, we present a study of bacteriorhodopsin demonstrating that UVRR can be used to determine time-resolved protein structural changes on the nanosecond and millisecond time scales. Nanosecond time-resolved spectra are obtained by initiating the BR photocycle with a visible pump pulse followed by a time-delayed UV probe pulse. A 240-nm probe pulse was used to study changes in tyrosine environment and protonation state in the BR → K transition. Millisecond time-resolved UVRR spectra are obtained by using a dual-beam, rapid-flow

† M.R. was supported by a fellowship from the Netherlands Organization for Scientific Research (NWO). This research was supported by grants from the National Science Foundation (CHE 91-20254) and the National Institutes of Health (GM 44801).

* To whom correspondence should be addressed.

‡ University of California at Berkeley.

§ Leiden University.

[1] Abbreviations: UVRR, ultraviolet resonance Raman; BR, bacteriorhodopsin; HEPES, 4-(2-hydroxyethyl)-1-piperazineethanesulfonic acid; FTIR, Fourier-transform infrared.

0006-2960/92/0431-5328$03.00/0

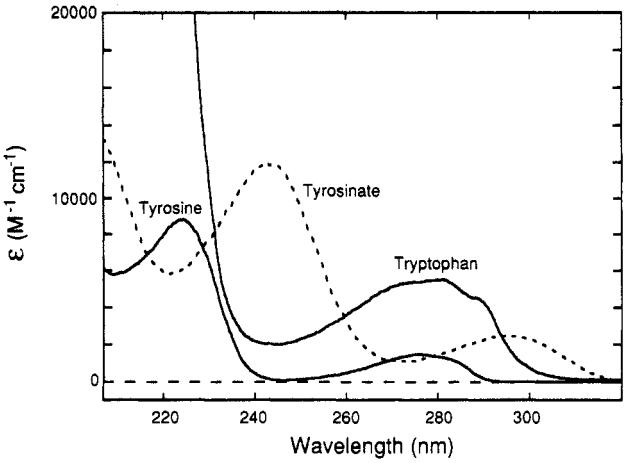

FIGURE 1: Absorption spectra of aromatic amino acids.

system. These data show that there is no change of the tyrosine ionization state in M_{412}. However, the millisecond difference spectra indicate that one or more *tyrosine* residues change environment in M_{412}. These results demonstrate the utility of time-resolved UVRR for studying protein structure and function.

Materials and Methods

Sample Preparation. Cultures of *H. halobium* (ET-1001) were grown and the purple membrane was purified according to previously published procedures (Braiman & Mathies, 1980). BR samples consisted of purple membrane fragments (150 μM) suspended in 3 M KCl and 1 mM HEPES (pH 7) at 25 °C. For Raman intensity measurements, samples were prepared as above but with 0.5 M KNO_3 added as an internal intensity standard. Addition of KNO_3 did not affect the absorption and Raman spectra. Aqueous solutions of 1.0 mM L-tyrosine (Sigma Chemical Co.) were prepared in 1 mM HEPES buffer (pH 7.0); tyrosinate solutions were prepared by raising the pH to 11.0 with KOH. *p*-Cresol crystals were dried by placing them in a desiccator over P_2O_5; 10 mM solutions were then prepared in methylene chloride, dioxane, or triethylamine (HPLC grade, Fisher) that had been dried over anhydrous $MgSO_4$.

L-Tyrosine-d_4 was prepared according to the procedure described by Winkel et al. (1989) and then incorporated into bacteriorhodopsin. Briefly, *Halobacterium halobium* (strain R_1S_9) was cultured from a standard growth medium (Gochnauer & Kusner, 1969) except that L-tyrosine-d_4 (0.2 g/L) was added and L-glutamic acid was replaced by L-glutamine. The extent of tyrosine-d_4 incorporation into the peptide chain was 95% as determined by GC/MS analysis (Raap et al., 1990).

Time-Resolved UV Raman Spectroscopy. Raman excitation at 240 nm was generated by focusing the 266-nm fourth harmonic from a Nd:YAG laser (DCR-2A, Quanta Ray) into a hydrogen-shifting cell operated at 80 psi. The Raman-shifted lines were separated by using a Pellin-Broca prism, and the desired 240-nm line was focused to a 0.5 × 0.25 mm rectangular spot on the sample. For the nanosecond experiments, the sample was flowed vertically through a wire-guided drip jet (Netto et al., 1990), forming a thin film (~100 μm thick) on which pump and probe beams were focused (see Figure 2A). For the millisecond experiments, sample was pumped through a capillary nozzle (1.4-mm i.d.), forming a horizontal jet (see Figure 2B). Backscattered Raman light was collected with quartz optics, dispersed by a Spex 1401 double spectrograph (11-cm^{-1} entrance slits), and detected with a PAR 1420

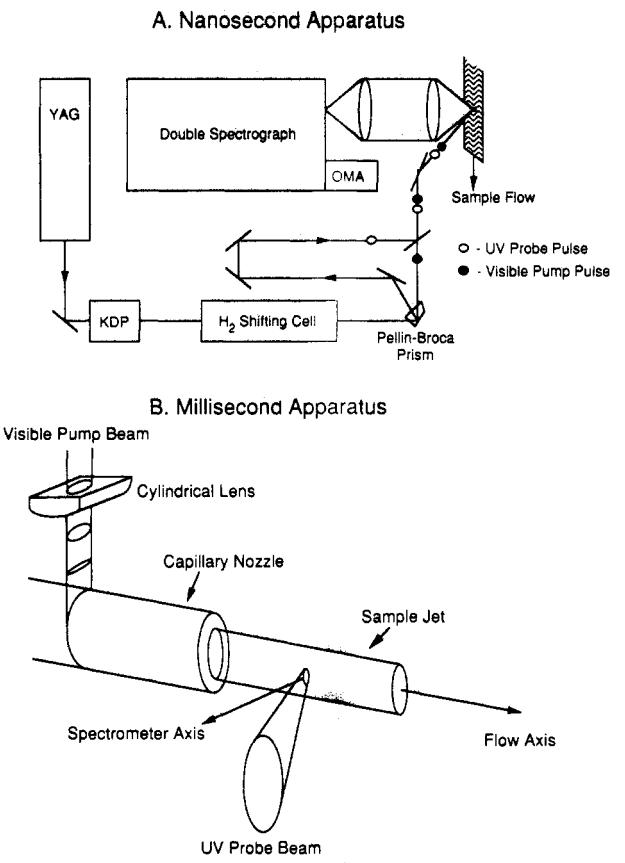

FIGURE 2: Schematic of the time-resolved UVRR apparatus for nanosecond (A) and millisecond (B) experiments. OMA = optical multichannel analyzer. KDP = potassium dihydrogen phosphate.

intensified reticon. Typically, seven to nine 20-min scans were averaged to give the desired signal-to-noise ratios. Fresh sample was introduced every 60 min to avoid artifacts due to sample photobleaching. Background scattering from the buffer was subtracted from all Raman spectra, and fluorescence backgrounds were removed using a cubic spline fitting routine. The Raman signals were linear in probe beam power from 1 to 15 mJ cm^{-2} $pulse^{-1}$. Using a typical power density of 3–5 mJ cm^{-2} $pulse^{-1}$, we calculate that ~30% of the protein molecules absorbed a UV photon. Using an estimated extinction coefficient of 28 000 M^{-1} cm^{-1} per protein (Becher et al., 1978) and unity quantum yield, this gives a photoalteration parameter (Mathies et al., 1976) of ~0.35. No vibrational bands from tyrosyl radicals at 1393, 1502, and 1552 cm^{-1} or photoproducts of tryptophan at 1522, 1593, and 1646 cm^{-1} (Johnson et al., 1986) were detected under these low-photolysis conditions. Furthermore, UV-pump, green-probe Raman experiments have shown that only a small fraction of the UV excitation is transferred to the chromophore (Netto et al., 1990).

Nanosecond time-resolved UVRR spectra were obtained by overlapping a 532-nm pump beam with the 240-nm UV probe beam. The pump pulse was spherically focused to a 1-mm spot superimposed on the optically delayed (10 ns) 240-nm probe. To quantitate the depletion of BR_{568} by the pump pulse, Raman scattering from BR_{568} at 1008 cm^{-1} was monitored using a 532-nm probe pulse (1 mJ/cm^2) delayed 10 ns from the separate 532-nm pump pulse. Figure 3 presents the depletion of BR_{568} as a function of pump power. The photochemistry begins to saturate beyond 20 mJ/cm^2 at which point the BR_{568} Raman signal at 1008 cm^{-1} is depleted by ~25%. This is presumably due to the photochemical reversibility of the BR → K transition. Since the photoproduct at 10 ns

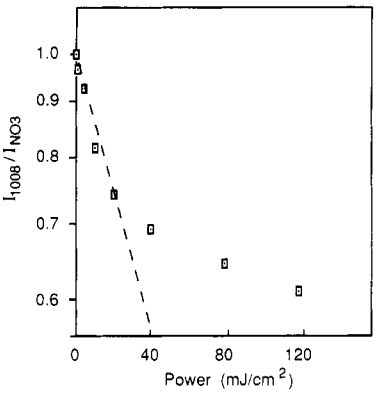

FIGURE 3: Depletion of BR_{568} by the 532-nm pump pulse as a function of power density. Visible Raman spectra were obtained by initiating the BR photocycle with a 532-nm pump pulse followed by a separate 532-nm probe pulse (1–2 mJ/cm^2) which was delayed 10 ns. A pump-only scan was subtracted from pump+probe scans (normalized to integration time) to correct for pump scattering. Pump+probe spectra were taken as a function of pump power, and the depletion of BR_{568} at each pump power was determined by measuring the BR_{568} scattering intensity at 1008 cm^{-1} relative to the nitrate scattering at 1049 cm^{-1}.

contains very weak scattering at 1008 cm^{-1} (Doig et al., 1991), the 25% depletion of the BR_{568} Raman signal is a good measure of the amount of photocycle intermediates produced by the pump pulse.

For millisecond time-resolved UVRR experiments, the BR sample was pumped from a 20-mL reservoir through a 1.4-mm i.d. capillary to form a horizontal jet with a linear velocity of 200 cm/s (see Figure 2B). The 514- or 568-nm cw pump beam was cylindrically focused (1.4-mm height, ~50-μm beam waist) onto the sample jet upstream from the probe. The time delay between pump and probe beams ranged from 0.04 to 10 ms (80 μm–2 cm). The polarization of the pump beam was set to 54.7° relative to the probe beam polarization to eliminate photoselection artifacts in the kinetics measurements. The depletion of BR_{568} by the pump beam was approximately linear in power up to 200 mW at 514 nm or 100 mW at 568 nm. Using a pump power of ~150 mW at 514 nm or 85 mW at 568 nm, the photoalteration parameter (Mathies et al., 1976) was ~1.1 assuming the maximum possible quantum yield of 0.6 (Schneider et al., 1989) and an extinction coefficient of 35 000 M^{-1} cm^{-1} at 514.5 nm or 63 000 M^{-1} cm^{-1} at 568 nm.

Results

Figure 4 presents nanosecond time-resolved UVRR spectra of BR with excitation at 240 nm. The pump+probe spectrum with 10-ns delay (Figure 4A) is probing a sample that consists of ~75% BR_{568} and ~25% photoproduct. Scattering from tyrosine at 1176 and 1206 cm^{-1} and from tryptophan at 1340, 1360, 1553, and 1618 cm^{-1} is evident. The probe-only spectrum in Figure 4B only contains scattering from BR_{568}. The difference spectrum between the pump+probe and probe-only (Figure 4C) provides no indication of a change in tyrosine, tryptophan, or tyrosinate scattering. Figure 4D presents a spectrum of tyrosinate in which the intensity has been scaled to that expected from the production of 1 equiv of tyrosinate per K formed (Ames et al., 1990). Comparison of Figure 4C and Figure 4D shows that the appearance of 0.25 equiv of tyrosinate would be detected with our signal-to-noise ratio.

For the millisecond time-resolved experiments, it was first necessary to quantitate the BR depletion and the M_{412} kinetics. Figure 5A presents millisecond time-resolved Raman data using a cw 457-nm probe and a 0.2-ms delay time which gives

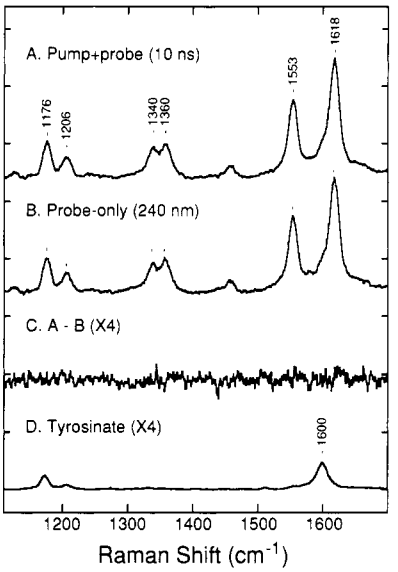

FIGURE 4: Nanosecond time-resolved UVRR spectra of BR. (A) Pump+probe spectrum obtained with a 240-nm probe pulse delayed 10 ns from the 532-nm pump pulse. (B) Probe-only spectrum obtained with just the 240-nm probe pulse. (C) Difference between pump+probe and probe-only spectra normalized to the 1553-cm^{-1} band and expanded 4-fold. (D) 240-nm Raman spectrum of 1 mM tyrosinate at pH 11.0 scaled to give the intensity expected from one tyrosinate per K species formed (Ames et al., 1990). The power density of the 240-nm probe was ~3 mJ/cm^2, and that of the 532-nm pump was ~20 mJ/cm^2.

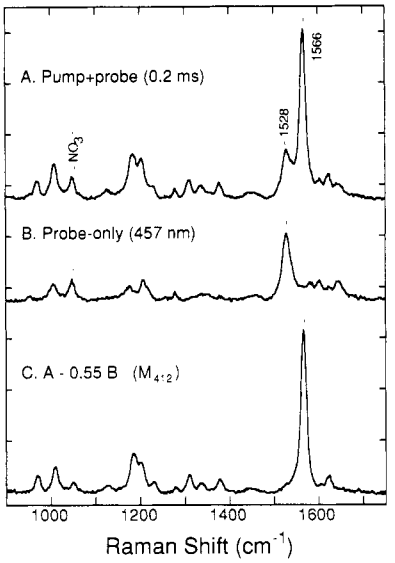

FIGURE 5: Time-resolved (0.2-ms delay) Raman spectra of BR with a 457-nm probe (30 mW) and 514-nm pump (150 mW). (A) Pump+probe spectrum. (B) Probe-only spectrum. (C) M_{412} spectrum obtained by subtracting 55% of the probe-only spectrum from the pump+probe spectrum.

maximal M_{412} concentration (Ames & Mathies, 1990; Varo & Lanyi, 1990). The apparent depletion of BR_{568} scattering at 1528 cm^{-1} relative to that from the probe-only is ~33%. Since the L and N intermediates both contribute ~10% to the scattering at 1528 cm^{-1} under these conditions (Ames & Mathies, 1990), the actual depletion of BR_{568} is probably closer to 45%. Consistent with these expectations, subtracting 55% of the probe-only spectrum from the pump+probe spectrum provided a relatively pure spectrum of M_{412} (Alshuth & Stockburger, 1986; Ames & Mathies, 1990; Braiman & Mathies, 1980). We therefore estimate that the relative pigment composition for a 0.2-ms delay under these conditions is 55% BR_{568}, ~30% M_{412}, and 10–15% L, N, and O.

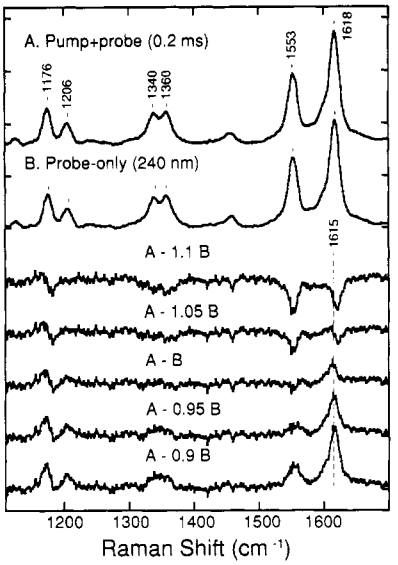

FIGURE 6: Millisecond time-resolved UVRR spectra of BR. (A) Pump+probe spectrum obtained with a 240-nm probe beam (3 mJ/cm^2) and a 150-mW, 514-nm pump beam. (B) Probe-only spectrum. Indicated amounts of the probe-only spectrum were subtracted from the pump+probe after normalizing each to the same 1553-cm^{-1} intensity. The difference spectra are expanded 4-fold for display. The delay time was determined by measuring the center-to-center distance between the pump and probe beams with a translation stage.

Figure 6 presents time-resolved UVRR spectra of BR with probe excitation at 240 nm and a 0.2-ms delay. The probe-only spectrum in Figure 6B only contains scattering from BR_{568}. Pump+probe and probe-only spectra were normalized to the intensity of the 1553-cm^{-1} band and then were subtracted using the indicated subtraction coefficients. Using a subtraction parameter of 100% produces a pure difference spectrum with no residual intensity at 1553 cm^{-1}, but positive peaks are observed at 1172 and 1615 cm^{-1} with possible derivative features centered at 1550 and 1176 cm^{-1}. A subtraction parameter of 100% was used for all subsequent difference spectra.

Figure 7 presents UVRR difference spectra at delay times ranging from 40 μs to 8 ms. At neutral pH (Figure 7A), the intensity changes at 1172 and 1615 cm^{-1} are found to follow the ~60-μs rise and ~2-ms decay of M_{412} (Ames & Mathies, 1990; Varo & Lanyi, 1990). However, assignment of the difference bands to the N_{550} intermediate cannot be ruled out because M_{412} and N_{550} both decay in about 2 ms at neutral pH (Ames & Mathies, 1990). The decay kinetics of M_{412} and N_{550} become clearly resolved at alkaline pH because the N_{550} decay slows to ~0.5 s at pH 9.5 (Fodor et al., 1988). Figure 7B presents millisecond UVRR difference spectra taken at pH 9.5. The difference bands still decay with an ~2-ms half-life. This shows that these signals must be assigned to M_{412}. The 1172- and 1615-cm^{-1} intensity changes will therefore be referred to as BR → M UVRR difference spectra.

Figure 8 compares the BR → M UVRR difference spectrum with spectra of tyrosine and tyrosinate. The tyrosinate spectrum in Figure 8B exhibits lines at 1174 and 1600 cm^{-1} while the tyrosine spectrum (Figure 8C) has lines at 1176 and 1615 cm^{-1}. The intensity of the tyrosinate spectrum has been scaled to that expected for 1 equiv of tyrosinate per M_{412} (Ames et al., 1990). The intensity scaling of the tyrosine spectrum is arbitrary. For 240-nm excitation, the tyrosine scattering is about 10-fold less intense than that from tyrosinate (Ludwig & Asher, 1988). Although the intensity change at 1615 cm^{-1} in the BR → M UVRR difference spectrum (Figure 8A) is close to that expected for tyrosinate, its frequency is

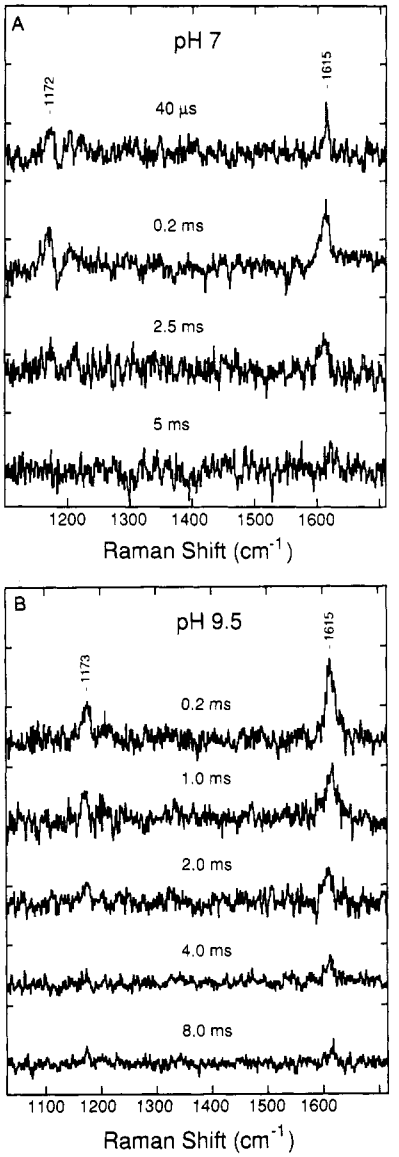

FIGURE 7: Time-resolved UVRR difference spectra of M_{412} at pH 7 (A) and pH 9.5 (B). Difference spectra were obtained as in Figure 6 at the indicated delay times. All other conditions were identical to those in Figure 6.

inconsistent with tyrosinate. The 1615-cm^{-1} frequency in the BR → M spectrum is more consistent with tyrosine scattering. However, the frequency of the 1172-cm^{-1} line in the BR → M spectrum is closer to that expected for tyrosinate (1174 cm^{-1}).

To determine the origin of the scattering in the BR → M UVRR difference spectrum, millisecond UVRR spectra were obtained on tyrosine-d_4-labeled BR. In tyrosine-d_4, the ν_{8a} and ν_{8b} vibrations downshift 25 cm^{-1} to 1590 and 1577 cm^{-1} (Figure 9), and the ν_{8b} mode is observed as a prominent shoulder. Also, the ν_{7a} and ν_{9a} vibrations disappear from our spectra and presumably downshift to below 1100 cm^{-1}. Figure 9E shows that the Raman-active ν_{8a} vibration of tyrosinate-d_4 downshifts 30 cm^{-1} to a single symmetric line at 1571 cm^{-1}. A tyrosine-d_4-labeled BR → M UVRR difference spectrum is presented in Figure 9C. The intensity change previously seen at 1615 cm^{-1} in the native pigment has shifted to 1590 cm^{-1} in Figure 9C with a shoulder at 1577 cm^{-1}. Also, the 1172 cm^{-1} band disappears, suggesting that it downshifted out of our spectral range. These shifts show that the scattering in the BR → M spectrum must arise from some form of tyrosine. The magnitude of the shift (25 cm^{-1}) as well as the presence

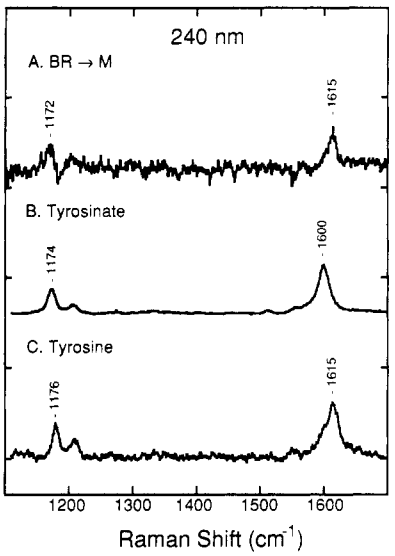

FIGURE 8: (A) BR → M UVRR difference spectrum (0.2-ms delay). (B) Raman spectrum of 1 mM tyrosinate at pH 11 scaled to represent the intensity expected for the appearance of 1 equiv of tyrosinate per M. (C) Raman spectrum of 1 mM tyrosine at pH 7 (240-nm excitation). Under these conditions, the tyrosine scattering is weak compared to that of tyrosinate. Thus, the tyrosine spectrum has been scaled by an arbitrary factor for display.

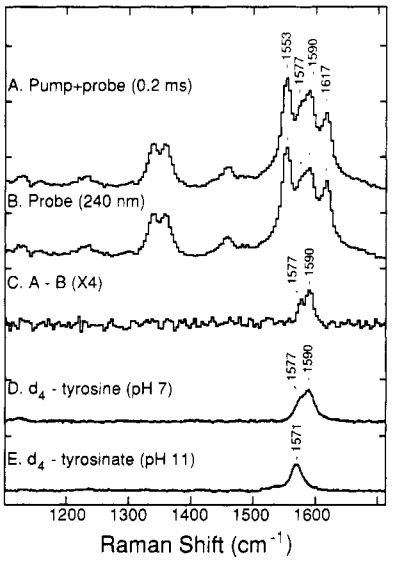

FIGURE 9: Time-resolved BR → M UVRR difference spectra of tyrosine-d_4-labeled BR. (A) Pump+probe spectrum obtained as in Figure 6A. (B) Probe-only spectrum. (C) Difference between pump+probe and probe-only spectra normalized to the 1553-cm^{-1} band and expanded 4-fold. (D) 240-nm Raman spectrum of 1 mM tyrosine-d_4 at pH 7. (E) 240-nm Raman spectrum of 1 mM tyrosinate-d_4 at pH 11 scaled to represent scattering from 1 equiv of tyrosinate in M_{412} (Ames et al., 1990). All other conditions are identical to those in Figure 8 except that the bin size in A–C has been increased 4-fold to provide a satisfactory signal-to-noise ratio.

of a shoulder at 1577 cm^{-1} indicates that the scattering in the BR → M UVRR difference spectrum is due to tyrosine rather than tyrosinate.

The sensitivity of tyrosine vibrations to hydrogen-bond strength provides an understanding of the 1172-cm^{-1} scattering in the BR → M UVRR difference spectrum. Figure 10 presents UVRR spectra of the tyrosine model compound *p*-cresol in a series of proton-accepting solvents of increasing hydrogen-bond strength: methylene chloride (K_a = 4.5; Ito, 1960), dioxane (K_a = 12.4; Bailey et al., 1968), and triethylamine (K_a = 295; Takahashi et al., 1967). The ν_{8a} vibration at 1615 cm^{-1} does not shift, but the 1174-cm^{-1} ν_{7a} mode

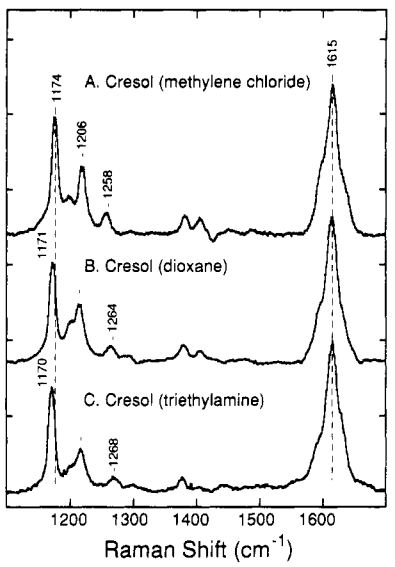

FIGURE 10: UVRR spectra (240-nm probe) of 10 mM *p*-cresol in (A) methylene chloride, (B) dioxane, and (C) triethylamine. All other conditions are identical to those in Figure 8.

progressively downshifts as the hydrogen-bond strength increases (to 1171 cm^{-1} in dioxane and to 1170 cm^{-1} in triethylamine). Conversely, the C–O stretching vibration (ν_{9a}) at 1258 cm^{-1} upshifts as a function of hydrogen-bond strength as observed previously (Takeuchi et al., 1989). This suggests that the downshifted line at 1172 cm^{-1} in the BR → M UV difference spectrum (Figure 8A) is due to the ν_{7a} vibration of one or more *tyrosine* residues which form a stronger phenolic hydrogen bond in M_{412} relative to BR_{568}.

Discussion

One goal of this study was to develop techniques for obtaining time-resolved UVRR spectra of the bacteriorhodopsin photocycle intermediates. Nanosecond UVRR spectra were obtained using 5-ns UV probe pulses from a Q-switched YAG laser which were optically delayed 10 ns from 5-ns pump pulses. Microsecond and millisecond UVRR spectra were obtained by flowing a horizontal jet of sample past spatially separated pump and probe beams, providing time delays from 40 μs to 10 ms. These experiments demonstrate that it is feasible to perform UVRR studies of protein structural changes with millisecond, microsecond, and even nanosecond time resolution.

Nanosecond UVRR of BR → K. Nanosecond UVRR spectra of the K intermediate were obtained to look for the involvement of tyrosinate in the BR → K transition. Our UVRR study, unlike previous FTIR studies of the BR → K transition, employed fully hydrated samples at room temperature which are the most native conditions for studying protein structure and function. FTIR studies of the BR → K transition revealed small intensity changes at 1277 cm^{-1} (C–O stretch) and 833 cm^{-1} (Fermi doublet), which were interpreted in terms of tyrosinate-185 protonation between BR_{568} and K (Braiman et al., 1988b). If a single tyrosine residue changed its protonation state in K, a tyrosinate band (ν_{8a}) at 1600 cm^{-1} should appear in the BR → K UVRR difference spectrum (Figure 4C) with the intensity shown in Figure 4D. *The BR → K difference spectrum provides no indication of a change of tyrosine protonation in the BR → K transition.* The frequencies of the IR-active C–O stretch and Fermi doublet modes of tyrosine are very sensitive to hydrogen-bonding environment (Takeuchi et al., 1989; this work) and are not unique to tyrosinate. Thus, the C–O stretch

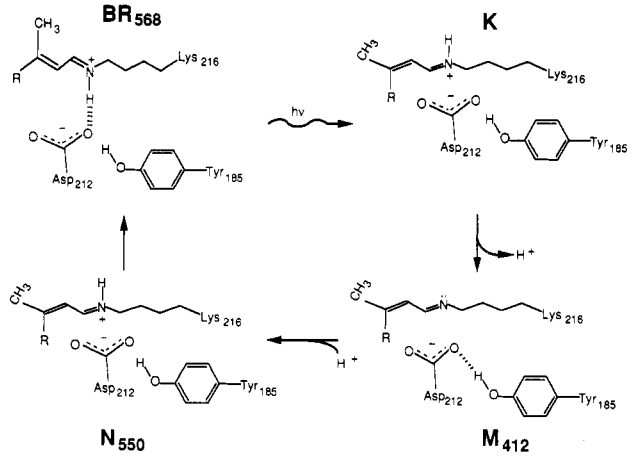

FIGURE 11: Schematic model of the hydrogen-bonding changes that occur in the BR photocycle.

and Fermi doublet frequency changes observed in the FTIR BR → K difference data may be due to an environmental change of a nonionized tyrosine residue. Consistent with this interpretation, recent FTIR studies on Asp-212 BR mutants have reassigned the 1277- and 833-cm^{-1} difference bands to a partially *protonated* form of Tyr-185 which forms a strong hydrogen bond with Asp-212 (Rothschild et al., 1990a).

Millisecond UVRR of BR → M. The absence of scattering at 1600 cm^{-1} in the BR → M UVRR difference spectrum indicates that there is no change in tyrosine ionization state between BR_{568} and M_{412}. It should be noted that if tyrosinate were present in both BR_{568} and M_{412} as suggested by FTIR studies (Braiman et al., 1988b), then there may be a cancellation of the tyrosinate signal in our BR → M difference spectrum. However, our UVRR studies on the BR_{568} → BR_{555} conversion do not support the presence of tyrosinate in BR_{568} (Ames et al., 1990). Our studies performed under native solvent conditions at room temperature are consistent with NMR studies of tyrosine in M trapped at low temperature (McDermott et al., 1991). Reproducible features are observed at 1172 and 1615 cm^{-1} in the BR → M UV Raman difference spectra that are due to *tyrosine* vibrations. The intensity changes most likely reflect an increase in resonance enhancement from one or more *tyrosine* residues in M_{412} due to a red-shift of the resonant L_a electronic transition. When M_{412} forms, the absorption increases at 240 and 296 nm, and this change was previously assigned to tyrosinate formation (Bogomolni et al., 1978; Hanamoto et al., 1984; Jang et al., 1990; Kalisky et al., 1981). However, this absorbance increase could also be caused by a red-shift of the $\pi \rightarrow \pi^*$ transitions of *tyrosine*. The $\pi \rightarrow \pi^*$ transitions of tyrosine derivatives red-shift in nonpolar solvents (Bailey et al., 1968) and in solutions with strong hydrogen-bond acceptors (Strickland et al., 1972). Also, Figure 10 shows that the ν_{7a} band downshifts in solvents that are stronger hydrogen-bond acceptors. *We therefore conclude that the features at 1172 and 1615 cm^{-1} in the BR → M UVRR difference spectrum are caused by a tyrosine residue that forms a stronger hydrogen bond with some residue in M_{412}.* Consistent with this conclusion, recent NMR studies have detected a change in tyrosine hydrogen bonding between BR_{568} and M_{412} (McDermott et al., 1991).

Figure 11 presents a structural model of BR which provides a molecular interpretation of these results. The proximity of Tyr-185 to Asp-212 in the retinal binding pocket (Henderson et al., 1990; Lin & Mathies, 1989) suggests that Tyr-185 forms a hydrogen bond with Asp-212. Asp-212 is thought to be ionized in BR_{568} as part of a complex counterion to the positively charged protonated Schiff base (Braiman et al., 1988a; De Groot et al., 1989; Subramaniam et al., 1990). The positively charged Schiff base in BR_{568} interacts electrostatically with ionized Asp-212. Photoisomerization of the chromophore and the subsequent deprotonation of the Schiff base in M_{412} remove the electrostatic stabilization of ionized Asp-212 by the Schiff base. This should permit Asp-212 to interact more strongly with Tyr-185 in M_{412}. The increased hydrogen-bond interaction between Tyr-185 and Asp-212 would then be responsible for the enhanced ν_{7a} and ν_{8a} scattering and for the shift of the ν_{7a} mode to 1172 cm^{-1}. This would suggest that Asp-212 remains ionized in M_{412}. The maintenance of this negative charge in the binding pocket is thought to be important for the reprotonation of the Schiff base during the M → N step (Mathies et al., 1991). Consistent with this explanation, the perturbed tyrosine signal decays during the M → N transition when the chromophore reprotonates (Fodor et al., 1988). It should be noted that our model disagrees with that of Braiman et al. (1988a), who suggest that Asp-212 undergoes a protonation change upon M formation. Further studies of time-resolved protein structural changes with UVRR employing different wavelengths and higher time resolution should reveal additional new information on the functional dynamics of proteins.

ACKNOWLEDGMENTS

We thank John Reilly for expert assistance in preparing bacteriorhodopsin samples.

REFERENCES

Alshuth, T., & Stockburger, M. (1986) *Photochem. Photobiol. 43*, 55–66.

Ames, J. B., & Mathies, R. A. (1990) *Biochemistry 29*, 7181–7190.

Ames, J. B., Bolton, S. R., Netto, M. M., & Mathies, R. A. (1990) *J. Am. Chem. Soc. 112*, 9007–9009.

Asher, S. A. (1988) *Annu. Rev. Phys. Chem. 39*, 537–588.

Bailey, J. E., Beaven, G. H., Chignell, D. A., & Gratzer, W. B. (1968) *Eur. J. Biochem. 7*, 5–14.

Becher, B., Tokunaga, F., & Ebrey, T. G. (1978) *Biochemistry 17*, 2293–2300.

Bogomolni, R. A., Stubbs, L., & Lanyi, J. K. (1978) *Biochemistry 17*, 1037–1041.

Braiman, M., & Mathies, R. (1980) *Biochemistry 19*, 5421–5428.

Braiman, M. S., Mogi, T., Marti, T., Stern, L. J., Khorana, H. G., & Rothschild, K. J. (1988a) *Biochemistry 27*, 8516–8520.

Braiman, M. S., Mogi, T., Stern, L. J., Hackett, N. R., Chao, B. H., Khorana, H. G., & Rothschild, K. J. (1988b) *Proteins: Struct., Funct., Genet. 3*, 219–229.

Dasgupta, S., Copeland, R. A., & Spiro, T. G. (1986) *J. Biol. Chem. 261*, 10960–10962.

De Groot, H. J. M., Harbison, G. S., Herzfeld, J., & Griffin, R. G. (1989) *Biochemistry 28*, 3346–3353.

Doig, S. J., Reid, P. J., & Mathies, R. A. (1991) *J. Phys. Chem. 95*, 6372–6379.

Dollinger, G., Eisenstein, L., Lin, S.-L., Nakanishi, K., & Termini, J. (1986) *Biochemistry 25*, 6524–6533.

Earnest, T. N., Herzfeld, J., & Rothschild, K. J. (1990) *Biophys. J. 58*, 1539–1546.

Efremov, R. G., Feofanov, A. V., Dzhandzhugazyan, K. N., Modyanov, N. N., & Nabiev, I. R. (1990) *FEBS Lett. 260*, 257–260.

Engelhard, M., Gerwert, K., Hess, B., Kreutz, W., & Siebert, F. (1985) *Biochemistry 24*, 400–407.

Engelhard, M., Hess, B., Emeis, D., Metz, G., Kreutz, W., & Siebert, F. (1989) *Biochemistry 28*, 3967–3975.
Fodor, S. P. A., Ames, J. B., Gebhard, R., van den Berg, E. M. M., Stoeckenius, W., Lugtenburg, J., & Mathies, R. A. (1988) *Biochemistry 27*, 7097–7101.
Gerwert, K., Hess, B., & Engelhard, M. (1990) *FEBS Lett. 261*, 449–454.
Gochnauer, M., & Kusner, D. (1969) *Can. J. Microbiol. 15*, 1157–1166.
Hanamoto, J. H., Dupuis, P., & El-Sayed, M. A. (1984) *Proc. Natl. Acad. Sci. U.S.A. 81*, 7083–7087.
Harada, I., & Takeuchi, H. (1986) *Advances in Spectroscopy, Volume 13: Spectroscopy of Biological Systems* (Clark, R., & Hester, R., Eds.) pp 113–175, Wiley, New York.
Harada, I., Yamagishi, T., Uchida, K., & Takeuchi, H. (1990) *J. Am. Chem. Soc. 112*, 2443–2445.
Harhay, G. P., & Hudson, B. S. (1991) *J. Phys. Chem. 95*, 3511–3513.
Henderson, R., Baldwin, J. M., Ceska, T. A., Zemlin, F., Beckman, E., & Dowing, K. H. (1990) *J. Mol. Biol. 213*, 899–929.
Herzfeld, J., Das Gupta, S. K., Farrar, M. R., Harbison, G. S., McDermott, A. E., Pelletier, S. L., Raleigh, D. P., Smith, S. O., Winkel, C., Lugtenburg, J., & Griffin, R. G. (1990) *Biochemistry 29*, 5567–5574.
Hildebrandt, P. G., Copeland, R. A., Spiro, T. G., Otlewski, J., Laskowski, M., & Prendergast, F. G. (1988) *Biochemistry 27*, 5426–5433.
Ito, M. (1960) *J. Mol. Spectrosc. 4*, 125–143.
Jang, D.-J., El-Sayed, M. A., Stern, L. J., Mogi, T., & Khorana, H. G. (1990) *Proc. Natl. Acad. Sci. U.S.A. 87*, 4103–4107.
Johnson, C. R., Ludwig, M., & Asher, S. A. (1986) *J. Am. Chem. Soc. 108*, 905–912.
Kalisky, O., Ottolenghi, M., Honig, B., & Korenstein, R. (1981) *Biochemistry 20*, 649–655.
Kaminaka, S., Ogura, T., & Kitagawa, T. (1990) *J. Am. Chem. Soc. 112*, 23–27.
Khorana, H. G. (1988) *J. Biol. Chem. 263*, 7439–7442.
Lin, S.-L., Ormos, P., Eisenstein, L., Govindjee, R., Konno, K., & Nakanishi, K. (1987) *Biochemistry 26*, 8327–8331.
Lin, S. W., & Mathies, R. A. (1989) *Biophys. J. 56*, 653–660.
Ludwig, M., & Asher, S. A. (1988) *J. Am. Chem. Soc. 110*, 1005–1011.
Mathies, R., Oseroff, A. R., & Stryer, L. (1976) *Proc. Natl. Acad. Sci. U.S.A. 73*, 1–5.
Mathies, R. A., Lin, S. W., Ames, J. B., & Pollard, W. T. (1991) *Annu. Rev. Biophys. Biophys. Chem. 20*, 491–518.
McDermott, A. E., Thompson, L. K., Winkel, C., Farrar, M. R., Pelletier, S., Lugtenburg, J., Herzfeld, J., & Griffin, R. G. (1991) *Biochemistry 30*, 8366–8371.
Miura, T., Takeuchi, H., & Harada, I. (1989) *J. Raman Spectrosc. 20*, 667–671.
Mogi, T., Stern, L. J., Marti, T., Chao, B. H., & Khorana, H. G. (1988) *Proc. Natl. Acad. Sci. U.S.A. 85*, 4148–4152.
Netto, M. M., Fodor, S. P. A., & Mathies, R. A. (1990) *Photochem. Photobiol. 52*, 605–607.
Ormos, P. (1991) *Proc. Natl. Acad. Sci. U.S.A. 88*, 473–477.
Raap, J., Winkel, C., de Wit, A. H. M., van Houten, A. H. H., Hoff, A. J., & Lugtenburg, J. (1990) *Anal. Biochem. 191*, 9–15.
Rava, R. P., & Spiro, T. G. (1985a) *J. Phys. Chem. 89*, 1856–1861.
Rava, R. P., & Spiro, T. G. (1985b) *Biochemistry 24*, 1861–1865.
Rothschild, K. J., Braiman, M. S., He, Y.-W., Marti, T., & Khorana, H. G. (1990a) *J. Biol. Chem. 265*, 16985–16991.
Rothschild, K. J., He, Y.-W., Mogi, T., Marti, T., Stern, L. J., & Khorana, H. G. (1990b) *Biochemistry 29*, 5954–5960.
Schneider, G., Diller, R., & Stockburger, M. (1989) *Chem. Phys. 131*, 17–29.
Song, S., Asher, S. A., Krimm, S., & Bandekar, J. (1988) *J. Am. Chem. Soc. 110*, 8547–8548.
Spiro, T. G., & Grygon, C. A. (1988) *J. Mol. Struct. 173*, 79–90.
Stoeckenius, W., & Bogomolni, R. A. (1982) *Annu. Rev. Biochem. 52*, 587–616.
Strickland, E. H., Wilchek, M., Horwitz, J., & Billups, C. (1972) *J. Biol. Chem. 247*, 572–580.
Su, C., Park, Y. D., Liu, G.-Y., & Spiro, T. G. (1989) *J. Am. Chem. Soc. 111*, 3457–3459.
Subramanian, S., Marti, T., & Khorana, H. G. (1990) *Proc. Natl. Acad. Sci. U.S.A. 87*, 1013–1017.
Takahashi, F., Karoly, W. J., Greenshields, J. B., & Li, N. C. (1967) *Can. J. Chem. 45*, 2033–2038.
Takeuchi, H., Watanabe, N., Satoh, Y., & Harada, I. (1989) *J. Raman Spectrosc. 20*, 233–237.
Toyama, A., Kurashiki, E., Watanabe, Y., Takeuchi, H., Harada, I., Aiba, H., Lee, B. J., & Kyogoku, Y. (1991) *J. Am. Chem. Soc. 113*, 3615–3616.
Varo, G., & Lanyi, J. K. (1990) *Biochemistry 29*, 2241–2250.
Wang, Y., Purrello, R., Jordan, T., & Spiro, T. G. (1991) *J. Am. Chem. Soc. 113*, 6359–6368.
Winkel, C., Aarts, M. W. M. M., van der Heide, F. R., Buitenhuis, E. G., & Lugtenburg, J. (1989) *Recl. Trav. Chim. Pays-Bas 108*, 139–146.